© <2021>. This manuscript version is made available under the CC-BY-NC-ND 4.0 license http://creativecommons.org/licenses/by-nc-nd/4.0/
The definitive publisher version is available online at https://doi.org/10.1016/j.jallcom.2021.162693

Multi-wavelength emission through self-induced defects in GaZnO microrods

M. Azizar Rahman[1, 2], Sajid Ali[1, a], Matthew R. Phillips[1], and Cuong Ton-That[1,*]

[1] *School of Mathematical and Physical Sciences, University of Technology Sydney, Ultimo, NSW 2007, Australia*

[2] *Bangladesh University of Engineering and Technology, Dhaka 100, Bangladesh*

[*]Corresponding author. Email: Cuong.Ton-That@uts.edu.au

Abstract

Multi-wavelength emission in wide bandgap semiconductors is commonly achieved through ternary alloying or quantum size effects. However, multi-wavelength emission within a single microstructure is highly challenging using these approaches. Here, we demonstrate that the luminescence wavelength within individual GaZnO microrods can be tailored via defect engineering. Fast chemical vapor growth of oxygen-rich ZnO microrods with Ga_2O_3 as an additive in the ZnO vapour leads to formation of a tapered morphology with graded distribution of Ga dopants, while the Ga incorporation does not significantly alter their crystal structure. With increasing Ga content from 1 to 6 at% from tip to base, the GaZnO microrods increase in diameter towards the substrate in accordance with the birth-and-spread mechanism. The local near-band-edge emission within single ZnO microrods, analyzed by nanoscale cathodoluminescence spectroscopy, exhibits a red shift of ~ 0.6 eV with increasing Ga content and exhibits signature characteristics of an excitonic emission. Density Functional Theory calculations reveal that the variation in the emission wavelength arises from bandgap narrowing due to the merging of the electronic states of Ga defect complexes with ZnO energy bands. The experimental and theoretical results demonstrate (i) the utility of using the self-regulation of defect compensation effects for band gap engineering and (ii) the possibility of multi-wavelength light sources within individual microrods.

Keywords: GaZnO microrod; wavelength-tunable emission; DFT calculations

[a] Current address: CAMD, Department of Physics, Technical University of Denmark, 2800 Kgs. Lyngby, Denmark

Introduction

Bandgap engineering is a common approach for tuning the optical and electronic properties of oxide and nitride semiconductors [1-3]. In solid state lighting and displays, multi-color emission with high efficiency is highly desirable but remains challenging because the band gaps currently available in elemental and binary compounds do not span the entire visible range. A conventional material engineering method to tune the bandgap is to alloy two or more semiconductors; however, the range of achievable bandgaps is limited because of the strict requirement of lattice matching in crystal growth. Here, we demonstrate that a wide range of optical bandgaps can be achieved within individual Ga-doped ZnO (GaZnO) microrods through band gap engineering methods that utilize the self-regulation of Ga doping induced charge compensation effects. These microrods exhibit intense near-band-edge emission owing to the tolerance of lattice mismatch afforded by microstructures.

Among wide bandgap semiconductors, ZnO continues to be of considerable research interest for applications in optical emitters due to its unique optoelectronic properties. The bandgap of ZnO and its optoelectronic properties can be tailored by incorporating dopants, such as Mg [4], Cd [5], and Be [6]. On the other hand, group III donors, such as Ga, are recognized as most effective dopants for controlling the n-type conductivity and electrical properties of the host material [7-9]. In ZnO, Ga favorably occupies substitutionally the Zn site (Ga_{Zn}), which acts as a shallow donor with a binding energy 55 meV [10]. For ZnO with high Ga doping levels, experimental measurements and first principle calculations have shown Ga donors could interact with acceptor-like defects, producing an abundance of Ga-related defect complexes, especially Ga_{Zn}-O_i and Ga_{Zn}-V_{Zn} pairs [11-13]. Moreover, these defect complexes, in sufficiently high concentrations, form a broad defect band near the valence band that can be

used to tailor the band gap of ZnO [13]. The influence of defect complex formation on the optical emission of GaZnO microwires was previously investigated in electroluminescence studies where the emission wavelength was found to vary between the microwires containing different Ga concentrations [14]. In this work, we demonstrate for the first time that multi-wavelength emission within individual GaZnO (GZO) microrods can be achieved via band gap engineering using the self-regulation of doping-induced defect compensation mechanisms. Such semiconductor microstructures with widely tunable optical bandgaps can be tailored for many new bespoke applications, in particular solid state lighting.

Unlike graded doping concentrations, typically achieved in the growth of semiconductor thin films, there have been few reports on bandgap grading within a single microstructure. The incorporation of Ga dopants into ZnO has been shown to cause either a blueshift or redshift in the near-band-edge (NBE) emission energy. The redshift results from the formation of defect complexes or localized band states at the degenerate doping level [8, 13], while the physical mechanism responsible for the composition-dependent blue shift of the ZnO UV luminescence is attributed to the Burstein-Moss effect [15, 16]. In this paper, we report the fabrication of $Ga_xZnO_{1-x}O$ microrods with a varying axial Ga concentration from x = 0 to 6 at% under an oxygen rich condition designed to favor the formation of Ga defect complexes [11]. Over this Ga concentration gradient, individual microrods exhibit a systematic red-shift in the excitonic emission of over 0.6 eV along their length from tip to base. Introducing dopants and point defects into the chemical vapor growth medium can also affect the morphology of ZnO microrod structures due to competition between lateral growth and axial growth [17-19]. Undoped ZnO crystals fabricated by vapor transport methods typically lengthen along their *c*-axis forming rod-like structures to reduce the contribution of the energetic polar (0001) facet and minimize the total surface energy. It has been shown that the

morphology of ZnO nanowires can be transformed via face-selective ion adsorption or modification of surface energies by addition of foreign ions during the growth phase [17, 19]. Significantly, the replacement of Zn surface sites with Ga during growth can passivate the ZnO (0001) polar surface, enhancing radial growth in the six $\{10\bar{1}0\}$ prismatic directions [19]. This principle is applied in the present work in which the rapid growth of single-crystalline tapered GZO microrods in the vapour phase is achieved. Correlative experimental analyses probing the local chemical composition, luminescence properties and defect structure along the length of the graded GZO alloy microrods, supported by computational defect simulation, are used to provide a model to explain the Ga-mediated modification of the excitonic emission.

Experimental section

GZO microrods were grown on polished silicon (100) wafers by a self-catalyzed chemical vapor deposition (CVD) in oxygen rich environment. Prior to the growth, a thin layer of zinc acetate was deposited on the substrate by spinning a layer of 20 mM of high purity (99.99%) $Zn(CH_3COO)_2$ H_2O in methanol. A layer of 15-20 nm thick ZnO film was produced after annealing at 400°C in Ar environment for 20 minutes. For CVD growth, a mixture of equal weights of oxide powder and graphite was used as the evaporating source. To grow GZO microrods, the oxide powder contains Ga_2O_3 30 wt%. The ZnO-coated substrates were placed upside down directly above the evaporation source. The source and substrate were mechanically transferred together to the high-temperature zone of a furnace at 1050ºC for 5 minutes under a constant oxygen flow rate of 20 sccm (oxygen pressure ~ 0.1 mbar), which facilitated the growth of GZO microrods through the carbothermal reduction of ZnO and Ga_2O_3. For TEM imaging, microrods were removed from the substrate by sonication and drop cast onto a 400 mesh Cu grid. Transmission Electron Microscopy (TEM) and Selected Area Electron Diffraction (SAED) analysis was carried out on a FEI Tecnai T20 TEM. Scanning Electron Microscopy (SEM) imaging and X-ray microanalysis were conducted on a Zeiss

Supra 55VP SEM equipped with an Energy Dispersive X-ray (EDX) analysis system. Cathodoluminescence (CL) was performed using a FEI Quanta 200 SEM equipped with a high-resolution Hamamatsu S7011-1007 CCD image sensor and a QE65000 Ocean Optics spectrometer. All luminescence spectra were corrected for the total response of the optical collection system. X-ray photoelectron spectroscopy (XPS) data were collected at a photon energy of 1486 eV on the soft x-ray spectroscopy beamline at the Australian Synchrotron.

Results and discussion

Fig. 1(a) shows a typical SEM image of tapered GZO hexagonal microrods with a diameter varying from ~ 0.5 μm in the tip region to ~ 6 μm at the base. The microrod length is > 25 μm. The surface of the tapered microrod is decorated with a series of regular facets normal to its axis accompanied by a number of steps where a large reduction in the width of the microrod occurs. EDX line scans across the width of a microrod at four different points along its length, presented in Fig. 1(b), reveal that the distributions of Ga and Zn are uniform across the width of the GZO microrod and that the Ga content gradually decreases as the diameter decreases from base to tip. A typical EDX spectrum from the microrod base shows characteristic X-ray emission peaks corresponding to Zn, Ga and O peaks (Supplementary Fig. 1S). EDX analysis reveals that the Ga content varies from ~ 6 at% at its base to 1 at% at its apex. This graded distribution of Ga is further confirmed by EDX Ga elemental mapping analysis that reveals a varying axial Ga content along the microrod (Fig. 1S). Fig. 1(c) shows the TEM image and its corresponding indexed SAED patterns in different regions of the GZO microrod tip. The diffuse streaks seen superimposed on the Bragg diffraction spots that extend in the direction perpendicular to the g⟨0001⟩ reciprocal lattice vector, shown in the zoomed-in image in the inset. The TEM and SAED results reveal that the GZO nanorods are single crystalline with a tapered growth direction along the *c*-axis. This result is entirely consistent

with the XRD patterns (Fig. 3S), which show the GZO microrods being predominantly oriented in the [0002] direction, and indicates that Ga incorporation up to 6 at% does not affect the *c*-axis growth habit of ZnO microrods. The chemical state of Ga dopants in the microrods were examined using XPS (Fig. 1d) that shows Ga $2p_{3/2}$ and Ga $2p_{1/2}$ peaks at 1117.8 and 1144.8 eV, respectively. The Ga $2p_{3/2}$ binding energy is close to that of Ga^{3+} ions in Ga_2O_3 single crystals at 1118.0 eV (also shown), indicating that Ga is incorporated into the microrods as Ga^{3+} ions without any other oxidation states. (The small difference in binding energy is due to the local environment of Ga in ZnO and Ga_2O_3.)

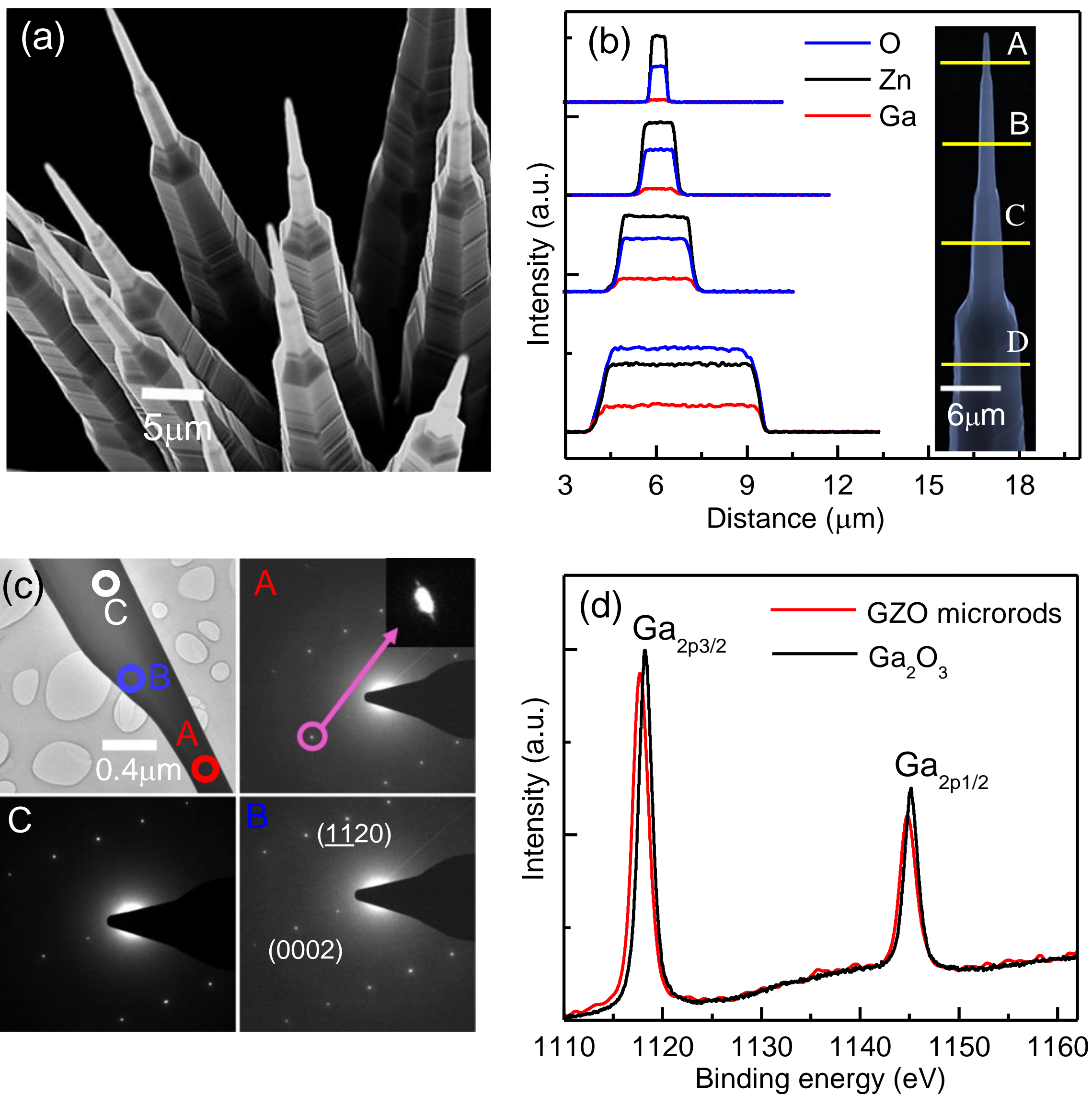

Figure 1. (a) SEM image of hexagonal GZO microrods showing tapered morphology when Ga was added to the growth environment. (b) EDX line scans (at 20 kV) along the dashed lines A, B, C and D across a microrod. The Ga content increases from ~ 1 at% at the microrod tip to ~6 at% at the base. (c) TEM image (taken at 200 kV) of the microrod tip and its corresponding indexed SAED patterns for different parts of the microrod. The diffraction streaks that extend in the direction perpendicular to the g<0001> reciprocal lattice vector confirms that the GZO nanorod is grown along the c-axis orientation. (d) XPS spectra of 2p for GZO microrod showing Ga $2p_{3/2}$ and Ga $2p_{1/2}$ electronic states, indicating that Ga is preferentially incorporated into the microrods as Ga^{3+} ions without any other oxidation states.

Addition of foreign ions during the growth phase of ZnO wires can alter the morphology of synthesized structures since their interaction with crystal facets influences the preferred growth direction and rates [17, 19]. A vapor-phase growth model for the tapered GZO microrods is illustrated in Fig 2(a). Pure ZnO microrods grown without Ga_2O_3 additive in the precursor display uniform diameter from top to base, whereas GZO microrods possess step-tapering morphology (Fig. 2S). Fig 2(b) shows the side view of GZO microrods revealing that they are constituted of faceted vicinal surfaces with several terraces along the sidewalls. The terrace size monotonically decreases from base to tip resulting the shrinkage of microrod diameter. Tapered ZnO structures have previously been observed with Ga [8], Sb [18], or Ge [20] being added to the precursor. Addition of Ga additive in the growth vapour does not perturb the growth *c*-axis orientation of microrods as shown in XRD analysis (Fig. 3S). Indeed, the Ga incorporation improves their crystallinity as the XRD (0002) peak in the GZO microrods become more dominant compared with their undoped ZnO counterparts. Undoped ZnO microrods have relatively small and non-tapered diameters, d ~ 150 – 200 nm. Since the polar (0001) face of pure ZnO possesses a much higher surface energy than the 6 prismatic {10-10}

faces, undoped microrods grow along the c-axis for the minimization of total surface energy.[19] Adding Ga to the growth vapor promotes the obelisk-like nucleation because Ga incorporation at Zn sites passivates dangling O bonds on the polar (0001) surface reducing its surface energy, so that the growth of GZO microrods is more favorable in the $[10\bar{1}0]$ directions [19]. The decrease in Ga concentration along to the microrod length correlates with reduction in the passivation of the (0001) surface, restoring its polar nature and enhancing a more needle-like structure to minimize the surface energy. The existence of facets along the tapering sidewalls of the GZO microrods suggests the formation of an Ehrlich-Schwoebel barrier as a result of dangling bonds at step edges [21]. This radial shell acts as a sink for adatoms, leading to the base region of GZO microrods being much larger than the tip. This type of growth can be described by the birth-and-spread mechanism controlled by impurity incorporation [22]. The tapering degree of the microrod can be characterized by angle φ, where $\tan\varphi = \frac{l}{L}$ (l is the size of a tapering step and L is the inter-step distance as illustrated in Fig. 2). The tapering degree is measured to be $\tan\varphi$ = 0.09 $\pm$ 0.01 in the tip region and 0.27 $\pm$ 0.03 at the microrod base. Dimensional analysis for > 10 microrods shows $\tan\varphi$ increases with the local Ga concentration (Fig. 2c), which is consistent with the Ga-mediated growth model described above as the Ehrlich-Schwoebel barrier effect becomes more pronounced with more Ga ions incorporated into Zn sites. This result agrees with previous findings that the tapering degree is highly sensitive to compositional change in Sn-doped ZnO nanowires grown by vapor-phase transport method [18].

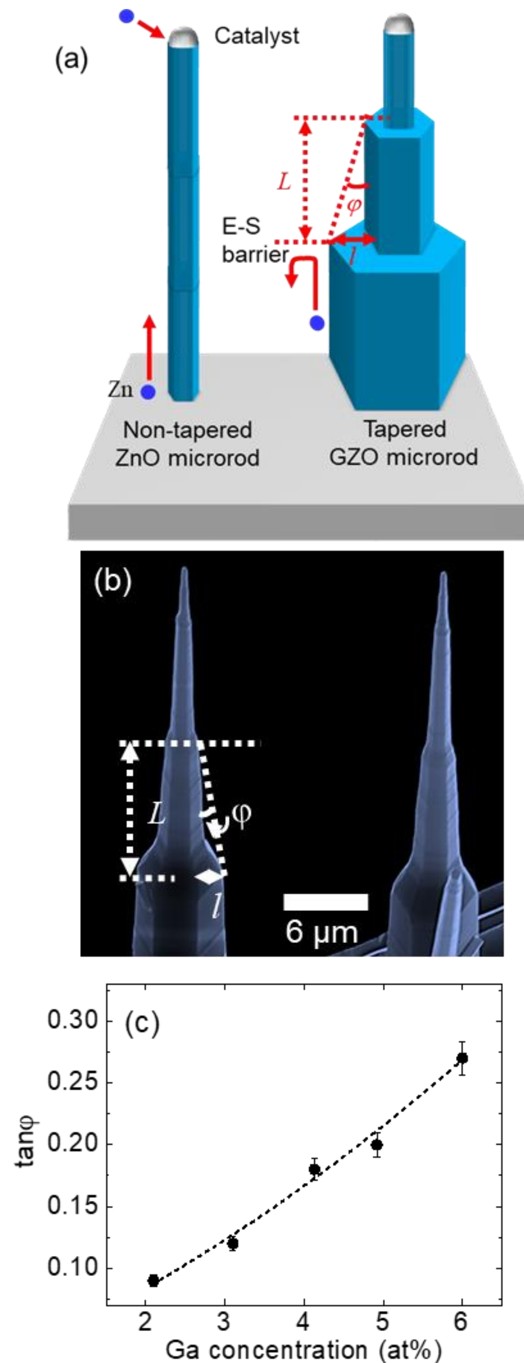

Figure 2. (a) Schematic of the growth mechanism for non-tapered ZnO and tapered GZO microrods. Adding Ga additive to the growth vapour promotes lateral growth and leads to the formation of an Ehrlich-Schwoebel barrier at the tapering steps. The tapering degree of the microrod is described by $tan\varphi = \frac{l}{L}$, where l is the size of a tapering step and L is the inter-step distance. (b) Side-view SEM image of tapered GZO microrods showing several steps along the sidewalls to accommodate the shrinking diameter from base to tip. (c) Variation of the tapering degree $tan\varphi$ with local Ga concentration in the GZO microrods. The error bars represent one standard error calculated from 10 microrods with similar dimensions.

Fig. 3(a) shows the CL spectra acquired at eight different points along the length of a single GZO microrod, which possesses a graded distribution of Ga from 1 at% at the tip to 6 at% at the base. These spectra, acquired at 80 K with a stationary e-beam, reveal that with increasing Ga content the NBE emission shifts to lower energy, broadens and becomes more intense. The CL peak energy and integrated intensity versus Ga content along the microrod are shown in Fig. 3(b). The NBE peak exhibits a monotonic redshift from 3.33 eV at the apex to 2.75 eV at the base, suggesting bandgap narrowing upon increasing Ga content along the microrod. Theoretical and experimental results have previously shown that the formation of $Ga_{Zn} - V_{Zn}$ and $Ga_{Zn} - O_i$ acceptor complexes is possible under oxygen rich conditions [11, 23]. For the GZO microrods, it is anticipated that the $Ga_{Zn} - V_{Zn}$ complex is formed in high concentrations since its formation energy is lower than that of Ga_{Zn} donors [11]. With high concentrations of Ga incorporated into the GZO microrods, the wavefunctions of the acceptor complex states will overlap, resulting in formation of an impurity band above the valence band maximum. This impurity band broadens with further increase in Ga concentration and eventually merges with the valence band maximum, forming a band tail state [24]. The direct transition between the conduction band and the valence band tail states leads to the redshift and broadening of CL emission peak. Fig. 4S shows the deep-level CL spectra of the ZnO and GZO microrods; the symmetrical, unstructured green luminescence band at 2.42 eV in ZnO is attributable to radiative recombination at V_{Zn} acceptors in earlier work [25]. This green emission is negligibly weak in the GZO microrods compared with the ZnO counterparts (Fig. 4S), which supports the passivation of isolated V_{Zn} defects when Ga is introduced into the growth vapor. Monte Carlo modelling using the CASINO simulation package [26] indicates the depth of maximum CL generation is ~ 450 nm at 10 kV and thus the CL generation volume is entirely contained within the GZO microrod. The NBE emission enhancement with

increasing Ga concentration from the tip to base of the microrod can thus be attributed to an increase in the densities of the Ga_{Zn} complexes.

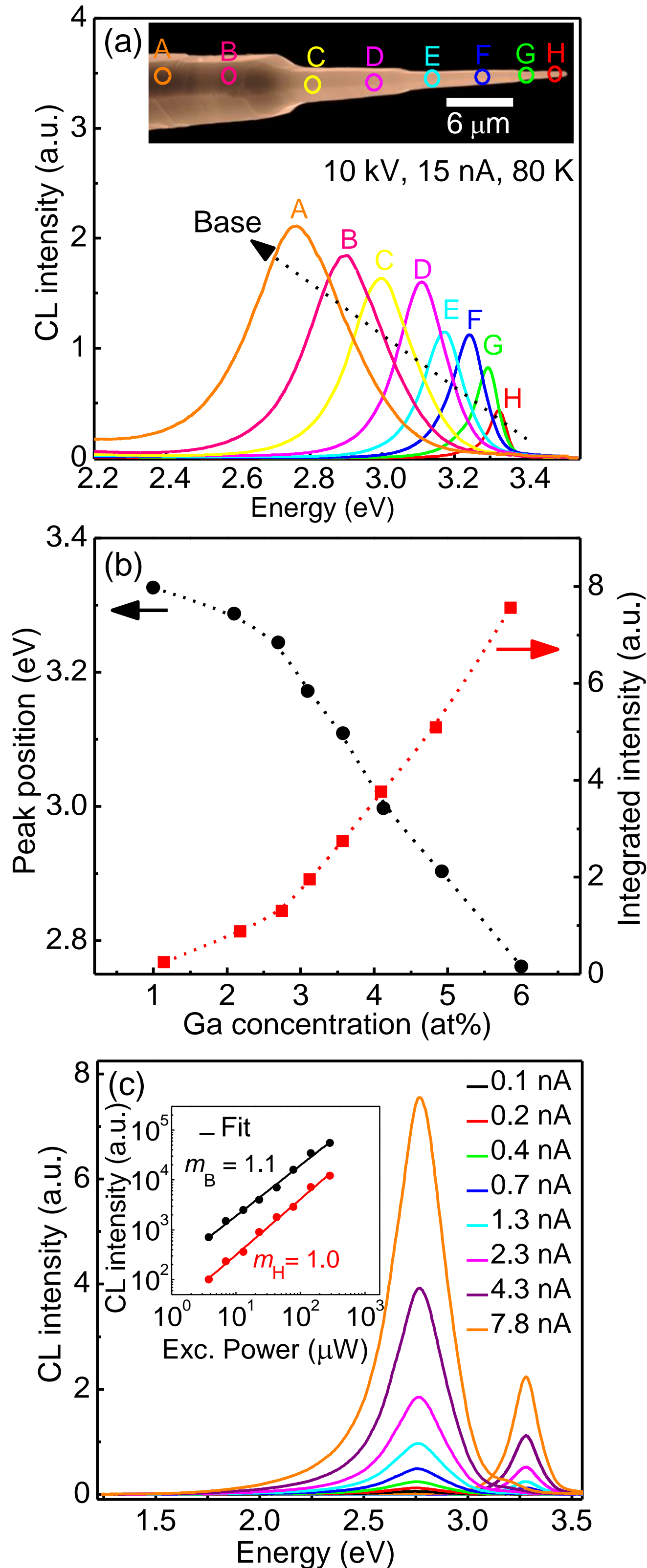

Figure 3. (a) CL spectra acquired at eight locations marked A to H along an individual GZO microrod from base to tip. (b) NBE peak energy and integrated intensity as functions of local Ga concentration in the microrod. As the Ga concentration increases from 1 to 6 at%, the NBE emission red shifts by ~ 0.6 eV and intensifies. (c) Excitation power-dependent NBE spectra

acquired at point B in the base and point H in the tip region of the microrod. Inset: log-log plots of NBE integrated intensities based on the power-law model yielding the power index m = 1.1 ± 0.04 and 1.0 ± 0.02 for locations B and H, respectively. These m values indicate that these emissions are of excitonic nature and not related to a lattice coupled defect.

To establish the physical mechanism responsible for the optical emission in the GZO microrods, excitation power density-dependent CL analysis was conducted. In this analysis the electron beam current (i.e. excitation power) was increased from 0.4 to 24 nA, while the beam energy was kept constant (E_B = 10 keV). Fig. 3(c) shows the excitation power-dependent CL spectra collected from the base (point B) and tip (point H) of the GZO microrod. Varying the excitation power in this range does not induce changes in NBE peak position or line shape. As shown in the inset of Fig. 3(c), the integrated NBE intensities follow the power law ($\mathrm{I}_{CL}\ \alpha\ \mathrm{P}^{m}$), where I_{CL} and P are the integrated emission intensity and CL excitation power, respectively [27]. Fitting the data to the power law yields m = 1.0 ± 0.02 and 1.1 ± 0.04 for the tip ([Ga] ≈ 1 at%) and base region ([Ga] ≈ 6 at%) of the graded GZO microrod, respectively. These almost linear behaviors with the exponent close to unity indicate that these emissions are of excitonic nature and not related to a lattice coupled defect [25]. Accordingly, the variation in the optical emission from the GZO microrods is attributed to a decrease in the optical bandgap mediated by the Ga dopant concentration.

To explain further the origin of the red-shift of NBE emission in the GZO microrod, Density Functional Theory (DFT) calculations were performed to model the variation of band gap with Ga content. All the calculations were undertaken using the Siesta [28] implementation of spin-unrestricted DFT with the Perdew Burke Ernzerhof approximation [29] to the exchange-correlation energy functional. The nucleus-electron interaction is represented by norm-conserving pseudopotentials calculated according to the method described by Troullier and Martins [30]. The electronic charge is represented by numerical pseudo-atomic orbitals

equivalent to a double-zeta plus polarization basis set. In Siesta, these orbitals are strictly confined to a cut-off radius determined by a single energy value representing the shift in orbital energy due to confinement. Here, a confinement energy value of 5mRy is used, which ensures sufficient convergence without excessive computational time. Pristine ZnO is first geometrically optimized using a 21 × 21 × 21 Monkhurst-Pack reciprocal space grids to a tolerance of 0.01 eV/Å. A large 3 × 3 × 2 supercell containing 36 ZnO units with a varying Ga concentration is used to realize defect-containing structures $Ga_xZn_{1-x}O-V_{Zn}$ and $Ga_xZn_{1-x}O-O_i$ (O_i is assumed to be at the octahedral site.) Fig. 4(a) shows the defect structure at x = 0.3 (See supplementary Fig. 5S for all defect structures with x ranging from 0 to 0.9.) For a supercell of this size, a reciprocal space grid of 7 × 7 × 10 is sufficient to ensure convergence of the total energy. The atoms in the defect structures are allowed to fully relax below a force tolerance of 0.03 eV/Å. These optimized structures are used to calculate the optical properties in random phase approximation using an optical mesh of 14 × 14 × 14 and an optical broadening of 0.02 eV.

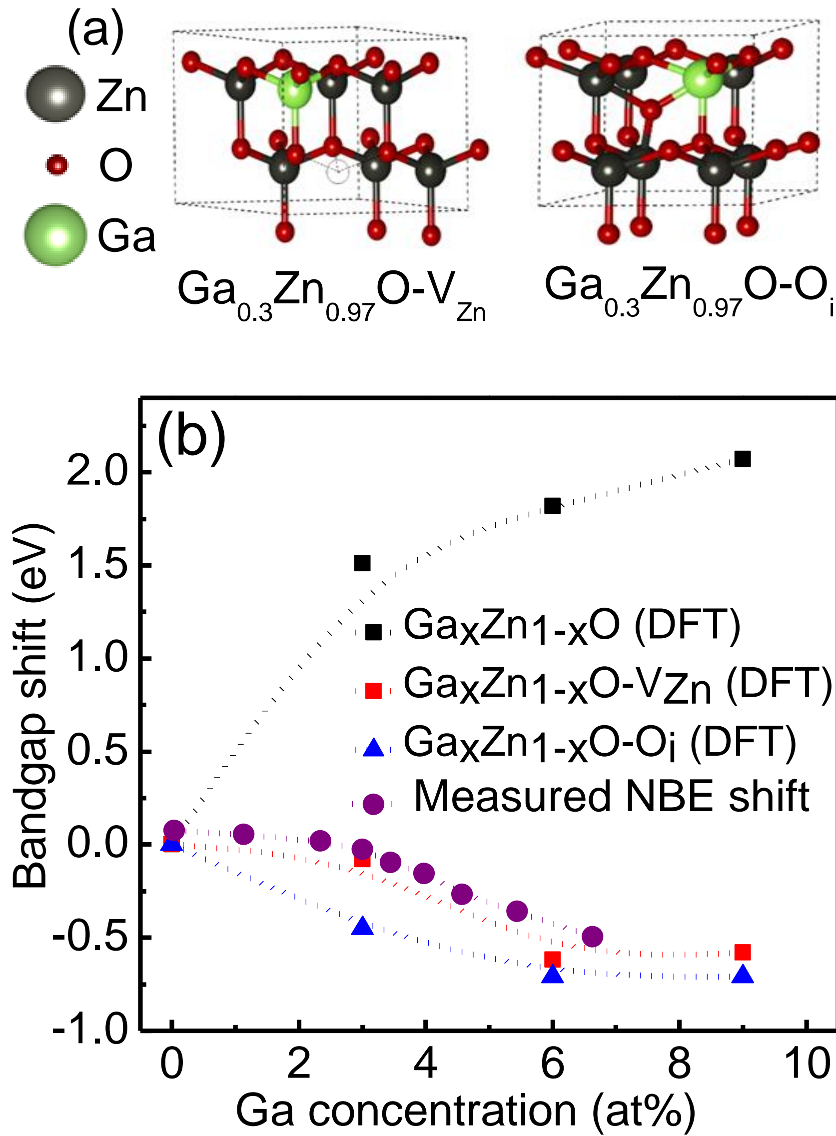

Figure 4. (a) A representative 2 × 2 × 1 supercell of $Ga_xZn_{1-x}O - V_{Zn}$ (left) and $Ga_xZn_{1-x}O - O_i$ (right) defect structures with the value of x = 0.3. (See supplementary material for the defect structures with all other x values.) For clarity these structures are cut from the larger 3 × 3 × 2 supercells used in the calculations. (b) Bandgap shift as a function of Ga concentration for $Ga_xZn_{1-x}O$ with and without defect complexes. The calculated $Ga_xZn_{1-x}O$ bandgap (black dotted line) increases with increasing Ga concentration due to the Burstein-Moss effect. In contrast, bandgap narrowing is found with the formation $Ga_xZn_{1-x}{-}V_{Zn}$ and $Ga_xZn_{1-x}{-}O_i$ acceptor complexes (red and blue dotted lines), in agreement with the measured NBE shift for the graded GZO microrod (purple solid circles).

The total density of states (DOS) of $Ga_xZn_{1-x}O$ with increasing concentration of Ga from x = 0 to 0.9 and for the $Ga_xZn_{1-x}-V_{Zn}$ and $Ga_xZn_{1-x}-O_i$ defect structures were calculated within the framework of DFT with Perdew–Burke Ernzerhof (PBE) functionals (see supplementary Fig. 5S). As shown in Fig. 5S (b, c), the valence band maximum (VBM) and conduction band minimum (CBM) of undoped $Ga_xZn_{1-x}O$ (x = 0) are contributed mostly by O *p* and Zn *s* states respectively, as expected. Using these DOS profiles, we analyze the bandgap shifts for the $Ga_xZn_{1-x}O$-V_{Zn} and Ga_xZn_{1-x}-O_i defect structures as a function of Ga concentration. The calculated bandgap shifts are displayed in Fig. 4(b), together with the observed shift in the excitonic emission of the GZO microrods. It is well known that DOS calculations based on PBE functionals generally underestimate the fundamental band gap.[31] However, since the aim of the calculations is to show the trend of bandgap with increasing Ga concentration rather than producing the absolute values, the DFT approach is adequate in describing the bandgap behaviour of the structures. Due to Coulomb interactions between the Ga_{Zn} donor and the acceptor-like V_{Zn} and O_i defects, the $Ga_xZn_{1-x}-V_{Zn}$ and $Ga_xZn_{1-x}-O_i$ structures are highly likely to form and act as bound complexes [11]. The DFT calculated increase of the $Ga_xZn_{1-x}O$ bandgap is found without these defect complexes, in agreement with previous studies.[32, 33] This increase in the bandgap is attributed to the Burstein-Moss band filling effect caused by the increase of carrier concentration at high Ga donor doping levels. On the other hand, bandgap narrowing is found with the formation of $Ga_{Zn}-V_{Zn}$ and $Ga_{Zn}-O_i$ complexes in $Ga_xZn_{1-x}O$.

For undoped $Ga_xZn_{1-x}O$ (x = 0) the valence band is composed mainly of O *p* states, while the hybridization of Zn *s*, *p* and O *p* states makes up the conduction band. In $Ga_xZn_{1-x}O-V_{Zn}$ and $Ga_xZn_{1-x}O-O_i$ complexes, the charge compensating Ga donor states and V_{Zn} and O_i acceptor states co-exist resulting in the narrowing of the bandgap as the conduction band minimum formed by hybridization of Ga-*p* and O-*p* states is pulled down in

energy [23, 31]. The VBM for $Ga_xZn_{1-x}O - O_i$ moves up in energy for all Ga x concentrations. Conversely, for $Ga_xZn_{1-x}O - V_{Zn}$ the VBM moves down in energy for Ga concentrations up to $x = 0.09$, where an upward shift of the VBM occurs due to complete compensation of Ga donors by V_{Zn} acceptors. The formation of Ga_{Zn}-O_i and Ga_{Zn}-V_{Zn} pairs generates an additional fully occupied impurity band above the VBM without changing the fundamental electronic properties of $Ga_xZn_{1-x}O$. With increasing Ga doping, the wavefunctions of the acceptor-like Ga_{Zn}-O_i and Ga_{Zn}-V_{Zn} pairs form a defect band that overlaps and ultimately merges with the valence band, resulting in a band tail state. Consequently, the carrier recombination in the $Ga_xZn_{1-x}O$ now occurs between the conduction band and the occupied impurity band rather than between the ZnO valence band and the Ga_{Zn} donor states in the conduction band. Additionally, since the width of the impurity defect band is dependent on the Ga x-fraction, increasing Ga concentration leads to narrowing of the band gap and the experimentally observed red shift of the excitonic emission.

Conclusions

Bandgap engineering in individual ZnO microrods with a graded distribution of Ga was studied. The optical emission from the microrod was found to intensify, broaden and red shift by 0.6 eV as the local Ga concentration increases from 1 to 6 at% along its length from tip to base. This emission from the microrod was confirmed to exhibit characteristics of a near band edge (NBE) excitonic emission. Theoretical DFT calculations indicate that the decrease of bandgap arises from the merging of the electronic states of Ga defect complexes with ZnO energy band edges. These results demonstrate the possibility of multi-wavelength light sources within a single GZO microstructure through band gap engineering that ultilizes the self-regulation of doping-induced defect compensation effects. Adding Ga additive to the growth precursor promotes the obelisk-like nucleation, increasing rod diameters and inducing the

tapering in GZO microrods. The mechanism for the tapering of microrod sidewalls in the <0001> growth direction is attributed to diminishing radial growth due to growth kinetics influenced by the reduction of Ga incorporation along the microrod length. The degree of tapering is found to directly correlate with the local Ga concentration within a microrod.

Acknowledgements

This work was supported under Australian Research Council (ARC) Discovery Project funding scheme (projects DP150103317 and DP210101146). M. Azizar Rahman acknowledges the financial support of Australian Government through the Research Training Program Scholarship. This research was partly undertaken on the Soft X-ray Spectroscopy (SXS) beamline at the Australian Synchrotron. Theoretical calculations were conducted with resources provided by National Computational Infrastructure (NCI) as well as Pawsey Supercomputing Centre with funding from the Australian Government and the Government of Western Australia. We thank Prof Michael Ford for useful discussions.

References

[1] E. Barrigon, M. Heurlin, Z.X. Bi, B. Monemar, L. Samuelson, Synthesis and Applications of III-V Nanowires, Chem. Rev., 119 (2019) 9170-9220.

[2] C.Z. Ning, L.T. Dou, P.D. Yang, Bandgap engineering in semiconductor alloy nanomaterials with widely tunable compositions, Nat. Rev. Mater., 2 (2017) 17070.

[3] Y.C. Cheng, H.C. Wang, H.C. Lai, S.C. Shi, C.C. Chen, Y.F. Yao, C.C. Yang, Wide range variation of resonance wavelength of GaZnO plasmonic metamaterials grown by molecular beam epitaxy with slight modification of Zn effusion cell temperatures, J. Alloys Compd., 870 (2021) 159434.

[4] P. Kumar, H.K. Malik, A. Ghosh, R. Thangavel, K. Asokan, Bandgap tuning in highly c-axis oriented Zn1−xMgxO thin films, Appl. Phys. Lett., 102 (2013) 221903.

[5] J. Jiang, L.P. Zhu, Y. Li, Y.M. Guo, W.S. Zhou, L. Cao, H.P. He, Z.Z. Ye, Band gap modulation of ZnCdO alloy thin films with different Cd contents grown by pulsed laser deposition, J. Alloys Compd., 547 (2013) 59-62.

[6] J. Khoshman, D. Ingram, M. Kordesch, Bandgap engineering in amorphous BexZnyO thin films, Appl. Phys. Lett., 92 (2008) 091902.

[7] C.S. Lee, B.T. Lee, S.H. Jeong, In-depth study on defect behavior and electrical properties in Ga-doped ZnO films by thermal-treatment under different chemical equilibrium, J. Alloys Compd., 818 (2020) 152892.

[8] X. Zhang, L. Li, J. Su, Y. Wang, Y. Shi, X. Ren, N. Liu, A. Zhang, J. Zhou, Y. Gao, Bandgap engineering of GaxZn1–xO nanowire arrays for wavelength-tunable light-emitting diodes, Laser Photonics Rev., 8 (2014) 429.

[9] A.T.T. Pham, D.V. Hoang, T.H. Nguyen, O.K.T. Le, D.P. Wong, J.L. Kuo, K.H. Chen, T.B. Phan, V.C. Tran, Hydrogen enhancing Ga doping efficiency and electron mobility in high-performance transparent conducting Ga-doped ZnO films, J. Alloys Compd., 860 (2021) 158518.

[10] B. Meyer, H. Alves, D. Hofmann, W. Kriegseis, D. Forster, F. Bertram, J. Christen, A. Hoffmann, M. Straßburg, M. Dworzak, Bound exciton and donor–acceptor pair recombinations in ZnO, Phys. Status Solidi (b), 241 (2004) 231-260.

[11] D. Demchenko, B. Earles, H. Liu, V. Avrutin, N. Izyumskaya, Ü. Özgür, H. Morkoç, Impurity complexes and conductivity of Ga-doped ZnO, Phys. Rev. B, 84 (2011) 075201.

[12] G.D. Yuan, W.J. Zhang, J.S. Jie, X. Fan, J.X. Tang, I. Shafiq, Z.Z. Ye, C.S. Lee, S.T. Lee, Tunable n-type conductivity and transport properties of Ga-doped ZnO nanowire arrays, Adv. Mater., 20 (2008) 168-173.

[13] C.S. Lee, C.H. Jeon, B.T. Lee, S.H. Jeong, Abrupt conversion of the conductivity and band-gap in the sputter grown Ga-doped ZnO films by a change in growth ambient: Effects of oxygen partial pressure, J. Alloys Compd., 742 (2018) 977-985.

[14] M.M. Jiang, G.H. He, H.Y. Chen, Z.Z. Zhang, L.X. Zheng, C.X. Shan, D.Z. Shen, X.S. Fang, Wavelength-Tunable Electroluminescent Light Sources from Individual Ga-Doped ZnO Microwires, Small, 13 (2017).

[15] Y. Liu, M. Jiang, G. He, S. Li, Z. Zhang, B. Li, H. Zhao, C. Shan, D. Shen, Wavelength-Tunable Ultraviolet Electroluminescence from Ga-Doped ZnO Microwires, ACS Appl. Mater. Interfaces, 9 (2017) 40743.

[16] T. Makino, Y. Segawa, S. Yoshida, A. Tsukazaki, A. Ohtomo, M. Kawasaki, Gallium concentration dependence of room-temperature near-band-edge luminescence in n-type ZnO: Ga, Appl. Phys. Lett., 85 (2004) 759-761.

[17] J. Joo, B.Y. Chow, M. Prakash, E.S. Boyden, J.M. Jacobson, Face-selective electrostatic control of hydrothermal zinc oxide nanowire synthesis, Nat. Mater., 10 (2011) 596-601.

[18] S. Li, X. Zhang, L. Zhang, Sb2O3-induced tapered ZnO nanowire arrays: the kinetics of radial growth and morphology control, J. Phys. Chem. C, 114 (2010) 10379-10385.

[19] J.I. Sohn, W.K. Hong, S. Lee, S. Lee, J. Ku, Y.J. Park, J. Hong, S. Hwang, K.H. Park, J.H. Warner, S. Cha, J.M. Kim, Surface energy-mediated construction of anisotropic semiconductor wires with selective crystallographic polarity, Sci. Rep., 4 (2014) 5680.

[20] Y. Liang, Ge-doped ZnO nanowire arrays as cold field emitters with excellent performance, Nanotechnology, 30 (2019) 375603.

[21] Z. Zhang, J.B. Yi, J. Ding, L.M. Wong, H.L. Seng, S.J. Wang, J.G. Tao, G.P. Li, G.Z. Xing, T.C. Sum, C.H.A. Huan, T. Wu, Cu-doped ZnO nanoneedles and nanonails: Morphological evolution and physical properties, Journal of Physical Chemistry C, 112 (2008) 9579-9585.

[22] K. Sangwal, Effects of impurities on crystal growth processes, Progress in Crystal Growth and Characterization of Materials, 32 (1996) 3-43.

[23] M.-H. Lee, Y.-C. Peng, H.-C. Wu, Effects of intrinsic defects on electronic structure and optical properties of Ga-doped ZnO, J. Alloys Compd., 616 (2014) 122-127.

[24] J. De-Sheng, Y. Makita, K. Ploog, H. Queisser, Electrical properties and photoluminescence of Te-doped GaAs grown by molecular beam epitaxy, J. Appl. Phys., 53 (1982) 999-1006.

[25] C. Ton-That, L. Weston, M. Phillips, Characteristics of point defects in the green luminescence from Zn-and O-rich ZnO, Phys. Rev. B, 86 (2012) 115205.

[26] C. Ton-That, M. Phillips, Cathodoluminescence microanalysis of ZnO nanowires, in: Semiconductor Nanowires, Elsevier, 2015, pp. 393-407.

[27] M.R. Phillips, H. Telg, S.O. Kucheyev, O. Gelhausen, M. Toth, Cathodoluminescence efficiency dependence on excitation density in n-type gallium nitride, Microsc. Microanal., 9 (2003) 144.

[28] J.M. Soler, E. Artacho, J.D. Gale, A. García, J. Junquera, P. Ordejón, D. Sánchez-Portal, The SIESTA method for ab initio order-N materials simulation, J. Phys. Condens. Matter, 14 (2002) 2745.

[29] J.P. Perdew, K. Burke, M. Ernzerhof, Generalized gradient approximation made simple, Phys. Rev. Lett., 77 (1996) 3865.

[30] N. Troullier, J.L. Martins, Efficient pseudopotentials for plane-wave calculations, Phys. Rev. B, 43 (1991) 1993.

[31] J. Wróbel, K.J. Kurzydłowski, K. Hummer, G. Kresse, J. Piechota, Calculations of ZnO properties using the Heyd-Scuseria-Ernzerhof screened hybrid density functional, Phys. Rev. B, 80 (2009) 155124.

[32] H.-C. Wu, Y.-C. Peng, C.-C. Chen, Effects of Ga concentration on electronic and optical properties of Ga-doped ZnO from first principles calculations, Opt. Mater., 35 (2013) 509-515.

[33] J. Zhao, X. Sun, H. Ryu, Y. Moon, Thermally stable transparent conducting and highly infrared reflective Ga-doped ZnO thin films by metal organic chemical vapor deposition, Opt. Mater., 33 (2011) 768-772.